Check for updates

The promotional effects of Mn on Ni/SiO$_2$ catalysts for CO methanation

Zhanggui Hou[1,3] · Yiming Chen[1] · Chuan Wang[1] · Xin Ma[1] · Hong Yang[2] · Wen Wang[1] · Yi Zhang[1,4]

Abstract

The Mn promoted Ni catalysts were developed and applied in CO methanation reaction. The 10%Ni/SiO$_2$ catalyst exhibits poor initial CO conversion (32.8%) and rapid deactivation with the highest methane selectivity during CO methanation reaction. In contrast, the Mn 4%Mn-10%Ni/SiO$_2$ catalyst shows dramatically increased initial CO conversion, which is up to 94.5% with 90.0% methane selectivity. Besides, the apparent activation energy, Ea value, of 4%Mn-10%Ni/SiO$_2$ was calculated to be 73.1 kJ/mol according to Arrhenius equation, which is much lower than that of 10%Ni/SiO$_2$ catalyst as 139.1 kJ/mol. Based on various characterization results, including in situ XPS and in situ CO-DRIFTS, it is found that the added Mn significantly improves the dispersion of the supported nickel, suppresses the sintering of nickel particles and forms more adsorbed CO species of three-fold carbonyl species, resulting in higher CO conversion and good stability during CO methanation reaction.

✉ Yi Zhang
    yizhang@mail.buct.edu.cn

1   College of Chemical Engineering, Beijing University of Chemical Technology, 15 Beisanhuan East Road, Beijing 100029, People's Republic of China

2   National Institute of Clean-and-Low-Carbon Energy, Beijing 102209, China

3   CNOOC Institute of Chemicals & Advanced Materials, China National Offshore Oil Corporation (CNOOC), Beijing 102209, People's Republic of China

4   Tarim University, Alar 843300, Xinjiang Uygur Autonomous Region, China

Introduction

In recent years, the synthetic natural gas (SNG) via methanation of synthesis gas has attracted much attention in academia and industry, with the increased demand of natural gas. Meanwhile, methanation has become an important pathway for the development of coal chemical industry, as the syngas can be obtained via gasification of coal [1, 2]. The various catalysts which contain different active metal components, such as Ni [3, 4], Ru [5] and Co [6], have been investigated for CO methanation.

Ni based catalyst along with porous materials support has been extensively applied in CO methanation, because of its high activity and low price [7–9]. However, Ni-based catalysts always suffer from deactivation due to the carbon deposition, sintering of metal particles and Ni loss during the methanation reaction [10, 11]. Therefore, how to alleviate deactivation phenomena has become a main research field for CO methanation process. Many reports suggested that the activity and stability of the supported Ni catalysts are strongly influenced by the amount of Ni metal loading [12, 13], the size of the dispersed Ni metal particles [14, 15], metal-support interactions [16, 17], and the composition of the support [18]. It is believed that the Ni dispersion and its chemical state on the support may play a key role in its catalytic performance [19]. It has been reported that the optimum electronic donor intensity and the nickel particle size on the catalyst can prevent the disproportionation of CO and suppress carbon deposition [20, 21]. Especially, sintering of the supported nickel, such as on Ni/SiO$_2$ catalyst, can accelerate the carbon deposition contributing to fast deactivation [21]. In addition, the formation of gaseous nickel-carbonyl species, which is influenced by the interaction between CO and Ni particles, can also lead to catalyst deactivation [11, 22, 23]. The mobile nickel-carbonyl species will cause the loss of active nickel species and accelerate the growth of the supported metal particles [24]. Moreover, the agglomeration and thermal degradation or sintering of the catalyst could rapidly decrease the surface area and hence, reducing the catalyst activity and lifetime [25, 26]. Therefore, suppressing the formation of surface nickel carbonyls and catalyst sintering could enhance the activity and stability for CO methanation over nickel based catalysts [27, 28]. Meanwhile, CeO$_2$ is often used as structural and electronic promoter or support, mainly because of its ability to improve dispersion of active components and to enhance the migration and exchange of oxygen species [4, 19]. Furthermore, it is reported that the addition of Mn to the catalysts could promote the dispersion of the supported metal and make the catalysts less prone to deactivation [29–32]. It is believed that addition of suitable metal oxide would enhance the activity and stability in CO methanation reaction.

Herein, the highly dispersed silica supported Ni-based catalysts were prepared by addition of Mn onto Ni/SiO$_2$ catalyst. The smaller Ni particle size and the different properties of nickel active phase were expected to improve the CO adsorption and reduced nickel sintering, contributing to high activity and excellent stability of Mn-Ni/SiO$_2$ catalyst in CO methanation. All obtained nickel catalysts

were characterized by XRD, TEM, H_2-TPR, XPS and in situ CO-DRIFTS, and the effects of the added Mn on the properties of nickel active phase as well as catalytic performance were investigated.

Experimental

Catalyst preparation

The Ni/SiO$_2$ catalyst was prepared by the incipient wetness impregnation method using commercial silica gel (SiO$_2$) as support (99.2%, Qingdao Haiyang Chemical Co., China; Specific surface area 455 m^2 g^{-1}, pore volume 1.06 cm^3 g^{-1}, average diameter of pore 9.6 nm). The metal loading of Ni was 10 wt%. Before the impregnation of SiO$_2$ with Ni precursors, the SiO$_2$ was pre-calcined at 400 °C for 2 h in the atmosphere of air. Then the aqueous solution (3.2 ml) of nickel nitrate (Ni(NO$_3$)$_2$·6H$_2$O, 1.65 g) was impregnated onto the pre-calcined SiO$_2$ support (3 g) by incipient-wetness impregnation method. After drying in air at 120 °C for 12 h, the sample was calcined at 400 °C for 2 h in the atmosphere of air. The obtained sample was denoted as 10%Ni/SiO$_2$.

The Mn-promoted Ni-based catalyst was prepared as described above by incipient wetness impregnations of aqueous solutions of nickel nitrate and Mn(NO$_3$)$_2$·4H$_2$O on silica gel supports. And the Mn loadings were set as 2, 4, 6, 8 wt%. The preparation procedure was as described for the unpromoted catalysts synthesized with the impregnation technique. The catalysts were marked as x%Mn-10%Ni/SiO$_2$, where x% is loading of Mn.

Catalyst characterization

X-ray diffraction (XRD) patterns of the passivated and used catalysts were recorded on D/max2500VB2+/PC X-ray diffractometer using graphite monochromatized Cu Kα radiation (λ=0.15406 nm) in the 2θ range from 10 to 90° with a scanning rate of 5° min^{-1}. The morphologies and sizes of the passivated and used samples were observed by transmission electron microscope (TEM, JEOL 2100F). The specimen was prepared by ultrasonically suspending the catalyst powder in ethanol. A drop of the suspension was deposited on a carbon-enhanced copper grid and dried in air.

H$_2$-Temperature programmed reduction (H$_2$-TPR) experiments were carried out in a quartz tube reactor using 0.1 g calcined catalysts. The reducing gas, a mixture of 10% H$_2$ diluted by Ar, was fed via a mass flow controller at 30 ml/min and the temperature was increased from 50 °C until 700 °C at a rate of 5 °C/min. The effluent of reactor passed through a 5 A molecular sieve trap to remove produced water, before reaching TCD.

The *in-situ* X-ray photoelectron spectroscopy (XPS) analysis was performed using a SHIMADZU AXIS Supra X-ray photoelectron spectrometer with an Al K$_α$ X-ray resource. The peaks were fitted by Gaussian–Lorentzian curves after Shirley or Tougaard background subtraction. All of the binding energies were

calibrated by the C1s peak at 284.8 eV. Prior to experiment, the pre-reduced samples were re-reduced in situ in a H_2 stream at 400 °C for 1 h in the catalytic chamber. After reduction, the sample was cooled down to room temperature under an N_2 atmosphere and transferred to the analysis chamber under vacuum conditions for measurements. After methanation reaction, the spent sample was also cooled down to room temperature under an N_2 atmosphere and transferred to the analysis chamber under vacuum conditions for measurements.

The in situ diffuse reflectance infrared Fourier transform spectra (in situ CO-DRIFTS) experiments were carried out on a NICOLET 6700 spectrometer. The pre-reduced sample (15 mg) was placed in an infrared cell with a ZnSe window and reduced in situ for 1 h in a H_2 gas flow at 400 °C and atmospheric pressure. Subsequently, the system was cooled to room temperature. After introduction of carbon monoxide at room temperature for 0.5 h, the catalysts were flushed by a N_2 stream for 1 h. All spectra were collected with a resolution of 4 cm^{-1} and accumulation of 32 scans.

Thermogravimetric (TG) analysis was conducted on a differential thermal analyzer (DTG-60, Shimadzu) and the experimental results were recorded and analyzed on a TA-60WS thermal analysis workstation. The sample of 5–10 mg was placed in a crucible. The temperature was increased from 25 °C to 800 °C with a heating rate of 10 °C/min, and the air flow rate was set to 50 ml/min.

Catalyst tests

Catalytic activity evaluation was carried out in a continuous-flow 9 mm I.D. fixed-bed quartz tubular reactor at ambient pressure. About 0.5 g catalysts diluted by 1.0 g quartz sand (20–40 mesh) were packed in reactor. Before the reaction, the catalysts were reduced at 400 °C for 10 h by pure H_2. The feed gas (H_2: 71.3%; CO: 23.7%; Ar: 5.0%) was introduced to start the reaction at 280 °C, 0.1 MPa, with GHSV = 16,000 h^{-1}. The effluent gas was on line analyzed using a gas chromatograph (GC-2014C, Shimadzu) equipped with a thermal conductivity detector (TCD) and flame ionization detector (FID).

The CO conversion (X_{CO}), CO_2, CH_4 and C_{2+} selectivity (S_{CxHy}) were estimated by the following equations:

$$X_{CO} = \left\{ \left(CO_{inlet} - CO_{outlet} \right) / CO_{inlet} \right\} \times 100\%$$

$$S_{CO2} = \left\{ \left(N_{CO2} \right) / \sum \left(x * N_{CxHy} \right) + N_{CO2} \right\} \times 100\%$$

$$S_{CxHy} = \left\{ \left(x * N_{CxHy} \right) / \sum \left(x * N_{CxHy} \right) + N_{CO2} \right\} \times 100\%$$

N_{CxHy} indicated the molar number toward a product with x carbon atoms.
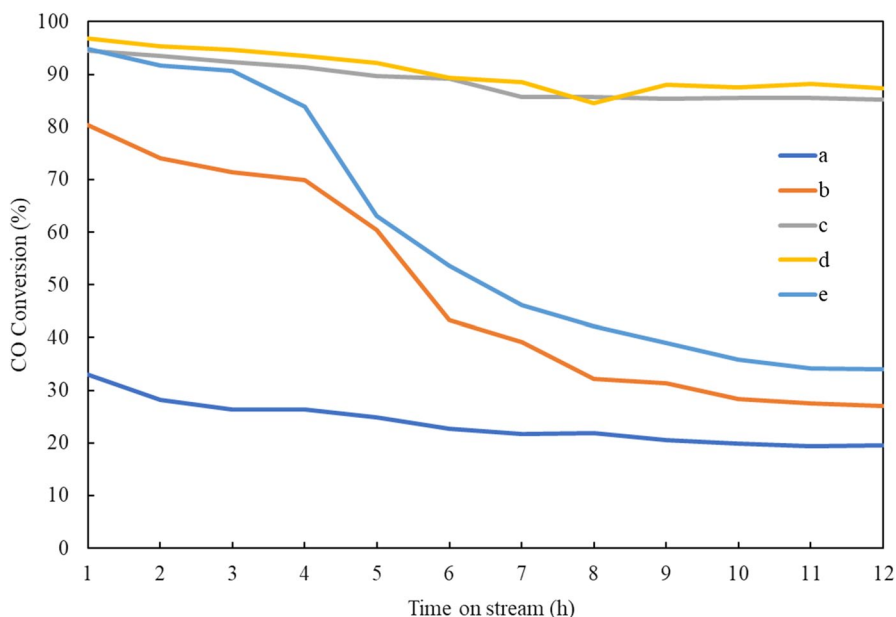
Fig. 1 Reaction performance of various catalysts. **a** 10%Ni/SiO$_2$, **b** 2%Mn-10%Ni/SiO$_2$, **c** 4%Mn-10%Ni/SiO$_2$, **d** 6%Mn-10%Ni/SiO$_2$, **e** 8%Mn-10%Ni/SiO$_2$. Reaction conditions: T=280 °C, P=0.1 MPa, GHSV = 16,000 h^{-1}, H$_2$:CO = 3:1

Table 1 Reaction performance and characterization results for various catalysts[a]

Catalysts	CO Conversion (%)[b]	Selectivity (%)[c]			Ni particle size (nm)[d]		Ni^0/Ni^{2+}[e]	
		CO$_2$	CH$_4$	C$_2$+	Reduced	Used	Reduced	Used
10%Ni/SiO$_2$	19.9	1.2	92.2	6.6	15.2	21.6	0.83	1.56
2%Mn-10%Ni/SiO$_2$	28.3	2.5	89.6	7.9	10.4	16.8	0.77	2.81
4%Mn-10%Ni/SiO$_2$	85.4	2.9	90.0	7.1	3.6	4.1	0.76	4.36
6%Mn-10%Ni/SiO$_2$	87.4	4.7	80.1	15.2	3.4	3.8	0.69	3.42
8%Mn-10%Ni/SiO$_2$	35.8	4.9	73.2	21.9	3.7	3.5	0.70	3.85

[a]Reaction conditions: T=280 °C, P=0.1 MPa, GHSV=16,000 h^{-1}, H$_2$:CO=3:1

[b]The CO conversion of the last hour

[c]Calculated by TCD and FID results

[d]Determined by TEM images

[e]Calculated by XPS results

Results and discussion

Reaction performance

The catalytic test results of all obtained catalysts are shown in Fig. 1 and Table 1.

The 10%Ni/SiO$_2$ catalyst exhibits poor initial CO conversion (32.8%) and rapid deactivation (19.9% CO conversion at last hour) with the highest methane selectivity (92.2%) during CO methanation reaction. In contrast, the Mn promoted 10%Ni/SiO$_2$ catalyst show dramatically increased initial CO conversion, which is up to 94.5% for 4%Mn-10%Ni/SiO$_2$ catalyst, as illustrated in Fig. 1. Meanwhile, the stability of 4%Mn-10%Ni/SiO$_2$ catalyst is significantly improved, whose CO conversion becomes steady from the 7th hour and is kept at 85.4% at the last hour as compared in Table 1. Furthermore, the 6%Mn-10%Ni/SiO$_2$ catalyst shows the highest CO conversion as 96.8% and the improved stability during the 12 h reaction, where the CO conversion of the last hour is kept at 87.4% as shown in Fig. 1. In contrast, further increasing Mn loading to 8% destroys the stability of the 8%Mn-10%Ni/SiO$_2$ catalyst. However, it is found that the methane selectivity decreases with the increased Mn loading as compared in Table 1. The lower CH$_4$ selectivity with the enhanced C$_2$+selectivity is obtained on the Mn promoted Ni/SiO$_2$ catalysts, especially for 6%Mn-10%Ni/SiO$_2$ and 8%Mn-10%Ni/SiO$_2$ catalysts, whose methane selectivity is as low as 80.1% and 73.2% respectively. It is reported that the CO inside the catalyst will form the nickel-carbonyl species on the active Ni particles, causing the sintering of the supported Ni particles [11, 24]. Meanwhile, the added Mn could suppress the formation of methane, promote the dispersion of the supported metal and make the catalysts less prone to deactivation [29–32]. Furthermore, as a promoter, Mn has demonstrated an increase in the selectivity toward longer chained hydrocarbons, inducing a characteristic increase in C$_5$+selectivity during Fischer–Tropsch synthesis (FTS) reaction [31, 32]. It is believed the added Mn could modify the properties of nickel active phase, resulting in significantly different reaction performance in CO methanation reaction.

Characterization of catalysts

XRD

XRD was used to investigate the bulk crystalline structure of all Ni-based catalysts. The XRD patterns of various passivated samples are shown in Fig. 2a. All samples exhibit a broad diffraction peak in the range between 10º and 30º which can be ascribed to the amorphous SiO$_2$. The peaks located at 44.5º, 51.7º, and 76.3º were the characteristic peaks of metallic Ni with a face-centered cubic structure (JCPDS# 87–0712). As shown in Fig. 2a, the unpromoted Ni/SiO$_2$ catalyst exhibits sharp and strong nickel peaks, and only metallic Ni is observed as the Ni species in all samples. In contrast, the nickel peaks of the Mn promoted Ni/SiO$_2$ catalyst becomes broader and weaker with the increased Mn loading. When the Mn loading is higher than 4%, the peaks of metallic nickel become too weak to calculate the crystalline size. This result suggests that the highly dispersed Ni catalysts were obtained due to the addition of Mn promoter [32], resulting in smaller crystalline size of the supported nickel, which would realize more active sites in the CO methanation reaction.

As shown in Fig. 2b., the XRD patterns of the spent catalysts illustrate that the sintering of the supported Ni only can be found on the unpromoted Ni/SiO$_2$ and the
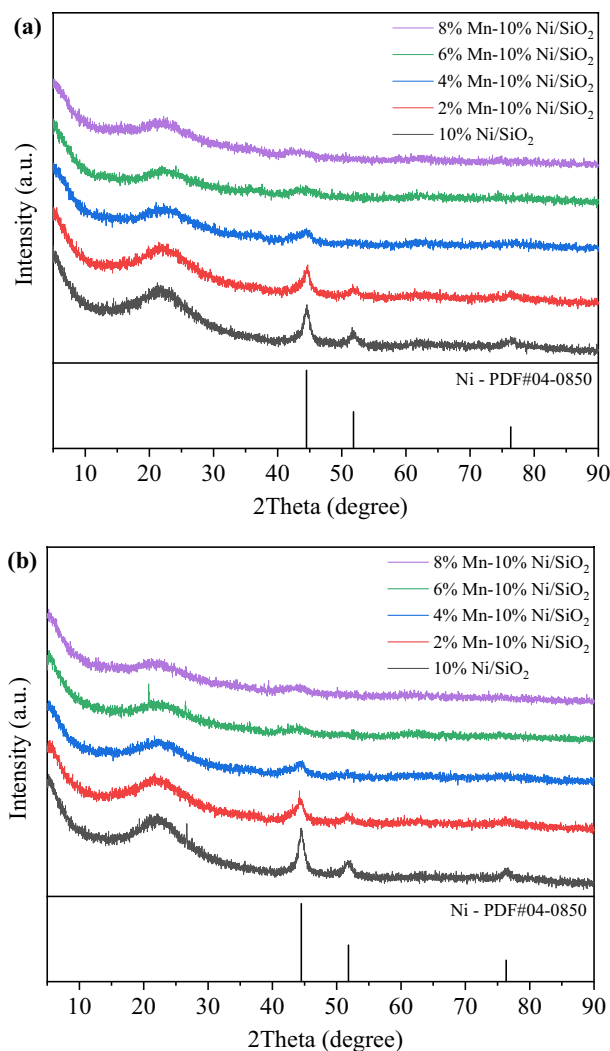
Fig. 2 XRD patterns of various Ni/SiO$_2$ with Mn promoter. **a** the reduced catalysts, **b** the used catalysts. Operating conditions: 2θ range from 10 to 90° with a scanning rate of 5 min^{-1}

2%Mn-10%Ni/SiO$_2$ catalysts after CO methanation reaction. The others still keep broad and weak nickel peaks after reaction, indicating the added Mn suppressed the sintering of the nickel particles contributing to the stability of the Mn promoted Ni/SiO$_2$ catalysts.

TEM and STEM

The TEM images of the reduced catalysts are shown in Fig. 3. It can be clearly seen that the supported nickel on the Ni/SiO$_2$ catalyst is clustered as 40–60 nm clusters
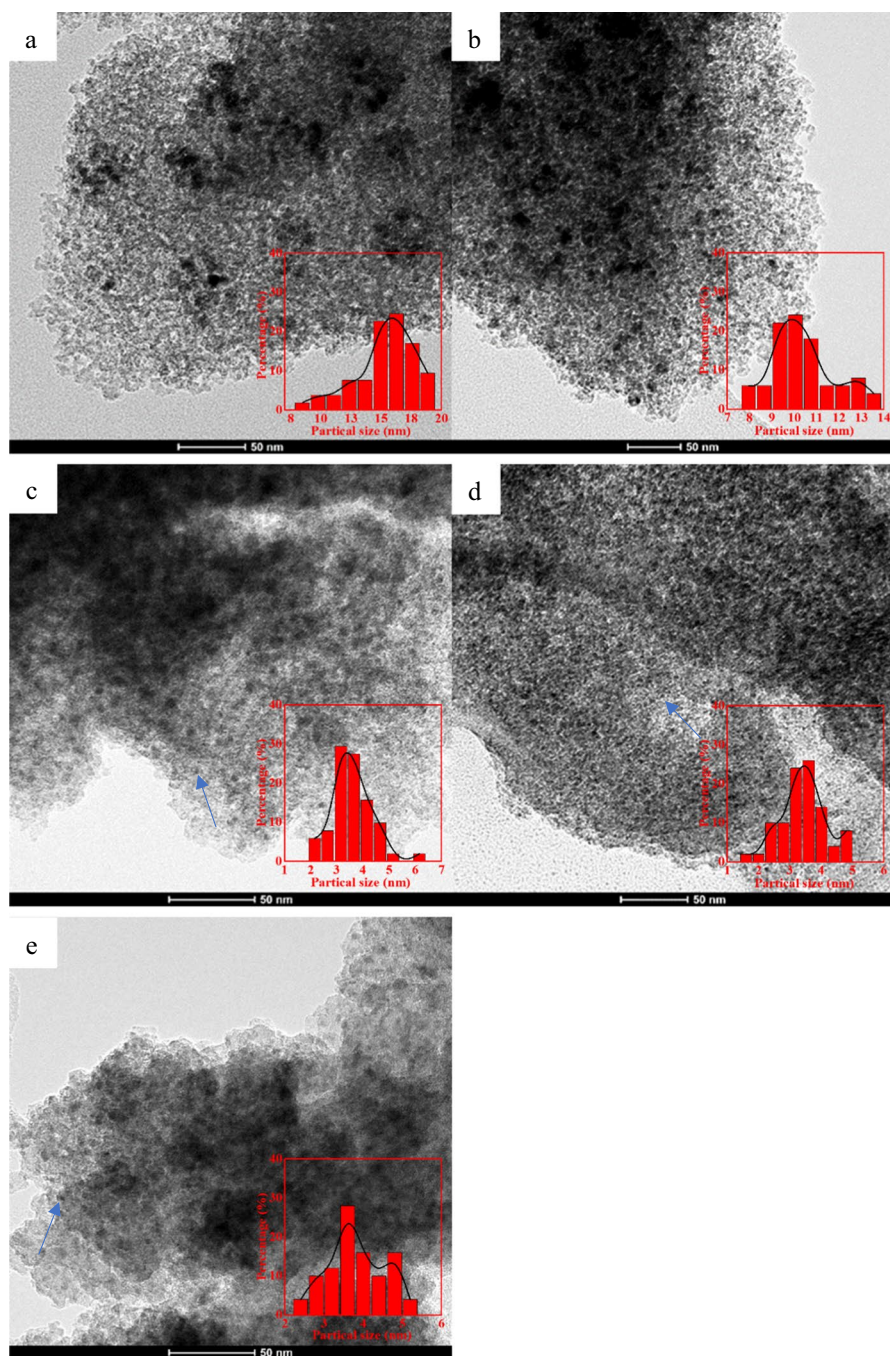
Fig. 3 TEM images of various reduced catalysts. **a** 10%Ni/SiO$_2$; **b** 2%Mn + 10%Ni/SiO$_2$; **c** 4%Mn + 10%Ni/SiO$_2$; **d** 6%Mn + 10%Ni/SiO$_2$; **e** 8%Mn + 10%Ni/SiO$_2$. Operating Conditions: carbon-enhanced copper grid and dried in air

(Fig. 3a), which contain many nickel particles of around 15 nm as compared in Table 1. In contrast, as shown in Fig. 3b~e for the Mn promoted Ni/SiO$_2$ catalyst, it is hard to find the clusters of the supported nickel particles, and the nickel particles are present separately and homogeneously distributed in the range of 3–10 nm on different Mn promoted catalysts (Table 1). These findings indicate that the added Mn significantly improved dispersion of the supported Ni on the Mn promoted Ni/SiO$_2$ catalysts, especially when Mn loading is higher than 4%.

For the used catalysts as shown in Fig. S1 and Fig. S2 (STEM images), the Ni/SiO$_2$ catalyst maintains the nickel cluster structure (Fig. S1a and Fig. S2a), as well as much larger nickel particles than fresh one, as shown in Table 1. And the 2%Mn-10%Ni/SiO$_2$ catalyst (Fig. S1b and Fig. S2b) also exhibits the enlarged nickel particles indicating the significant sintering of the supported nickel during the reaction. Therefore, it is considered this should be the reason of deactivation during CO methanation over Ni/SiO$_2$ and 2%Mn-10%Ni/SiO$_2$ catalysts. However, from 4%Mn-10%Ni/SiO$_2$ catalyst, the nickel particles of these three catalysts well suppress sintering and keep homogeneous distribution, as compared in Table 1. It is believed that the addition of Mn obviously promoted the dispersion of the supported Ni, contributing to the stability during CO methanation.

H$_2$-TPR and in situ XPS

The H$_2$-TPR profiles of the obtained catalysts are illustrated in Fig. S3. For the unpromoted Ni/SiO$_2$, there are two main reduction peaks in the H$_2$-TPR profile. The broad peak located at the low temperature region (240–350 °C) are assigned to the free NiO species on the surface of catalysts or easily reducible species, and the peak around 400 °C suggests the existence of NiO particles that strongly interact with the support on this 10%Ni/SiO$_2$ sample [33]. As the manganese oxide would be reduced below 400 °C [29], the first nickel reduction peak overlaps the reduction peaks of MnOx for the Mn promoted catalysts. However, the second nickel reduction peak clearly illustrate the reduction behavior of different Mn promoted catalysts. It can be seen that the second reduction peaks of the supported nickel are moved to higher temperature by the increased Mn loading. Therefore, it suggests that the addition of Mn onto Ni/SiO$_2$ catalyst enhances the interaction between the supported nickel and silica support, resulting in more smaller nickel particles as proved by TEM and XRD.

To clarify the nickel active phase, in situ XPS was applied to probe the chemical states of surface Ni species in all catalysts. As shown in Fig. 4a, for 10%Ni/SiO$_2$ catalyst, the binding energy at 871.0 and 853.9 are assigned to $Ni^0_{2p1/2}$ and $Ni^0_{2p3/2}$, while the binding energy at 875.2 and 856.8 are $Ni^{2+}_{2p1/2}$ and $Ni^{2+}_{2p3/2}$, respectively. And all peaks with orange line are satellite peaks of Ni [11, 34]. For the Mn promoted catalysts, the nickel species have similar BE values to that of 10%Ni/SiO$_2$ catalyst which has the largest Ni particle size, suggesting that the Mn species donate electrons to nickel species and decrease the BE values of nickel species [29, 34, 35]. Furthermore, as compared in Fig. 4a and Table 1, for the Mn promoted catalyst, the Ni^0/Ni^{2+} ratio decreases with the increased Mn loading, suggesting that the reduction of the supported Ni is prevented by the added Mn as proved by H$_2$-TPR.
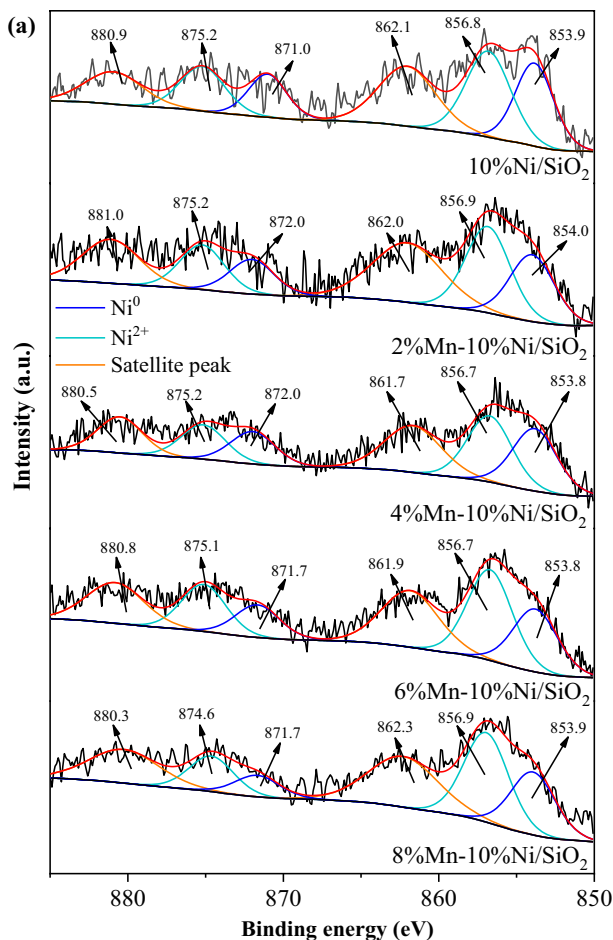
Fig. 4 Ni 2p XPS spectra of Ni/SiO$_2$ with different Mn loading. **a** reduced catalysts, **b** used catalysts. Operating Conditions: Al K$_\alpha$ X-ray resource

The XPS profile of various spent catalysts are shown in Fig. 4b. For 10%Ni/SiO$_2$ catalyst, the peak of Ni$^0_{2p3/2}$ shift to lower BE values than that of the reduced catalyst, indicating high electron density of large nickel particles induced by sintering during reaction [29, 34], as proved by XRD and TEM. On the other hand, the NiCx species [36] can be found on the 6%Mn-10%Ni/SiO$_2$ and 8%Mn-10%Ni/SiO$_2$ catalysts. It is considered that the higher loading of Mn improved the formation of NiCx resulting in deactivation during CO methanation reaction. Meanwhile, as compared in Table 1, the Ni^0/Ni^{2+} ratio of the spent catalysts is higher than that of the reduced one, implying the reduction of the supported nickel during reaction as previously reported [37]. Therefore, it is believed that the dynamic reduction process during methanation reaction could influence the
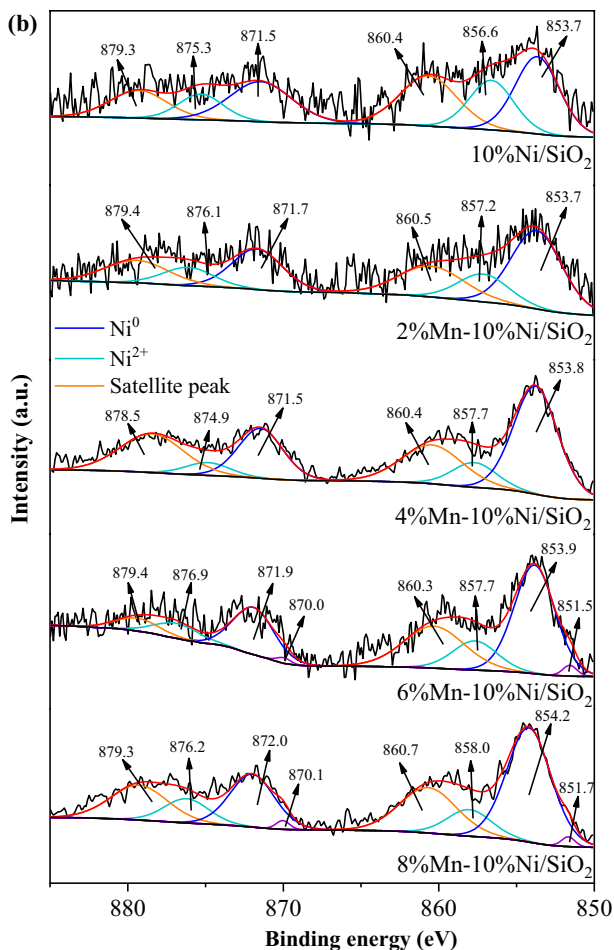
Fig. 4 (continued)

properties of nickel species and induce sintering or carbonization of the supported nickel, resulting in deactivation of Ni based catalysts.

CO-DRIFTS and TGA

As reported, different adsorbed CO species on the catalysts would determine the activity of the catalysts in methanation reaction [11, 29, 37, 38]. In order to further investigate the adsorbed CO species on the different catalysts, in situ CO-DRIFT were performed on all catalysts, and the results are shown in Fig. 5.

As reported, the adsorbed CO bands on nickel-based catalyst are in the range of 2100–1750 cm^{-1}, in which the bridge-bound CO (1950–1750 cm^{-1}) is associated to CO adsorption on the close-packed Ni sites, whereas linear-bound CO (2100–1950 cm^{-1}) refers to CO connected on Ni defect sites [11, 34, 39]. As
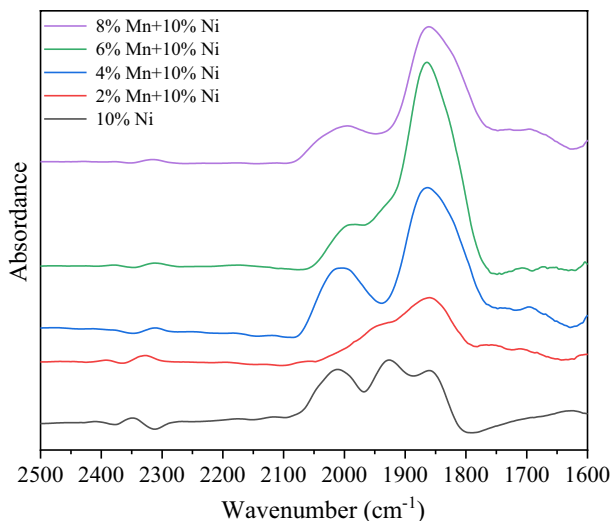
Fig. 5 In situ CO-DRIFT spectra of various Mn promoted Ni/SiO$_2$ catalysts. Operating Conditions: 4 cm^{-1} and 32 scans

shown in Fig. 5, for 10%Ni/SiO$_2$ catalyst, the broad CO bands from 1965 cm^{-1} to 2064 cm^{-1} can be attributed to Ni(CO)$_x$, which is linearly/terminally adsorbed CO atop a single nickel atom [11, 24, 39]. In addition, the adsorbed CO band located at 1931 cm^{-1} should be attributed to the bridge-band CO on the close-packed Ni sites [11, 34]. And the CO band at 1857 cm^{-1} can be attributed to the three-fold carbonyl species, i.e. CO species bound to three neighbouring Ni atoms, which are advantageous to the CO hydrogenation [11, 39].

However, for the Mn promoted catalysts, the CO band of three-fold carbonyl species (1857 cm^{-1}) is significantly improved as illustrated in Fig. 5, contributing to higher initial CO conversion as shown in Fig. 1. Meanwhile, it is believed that the higher amount of three-fold carbonyl species on the Mn promoted catalysts would improve the selectivity of C$_2$+hydrocarbon as compared in Table 1. Besides, it is considered that the lower ratio of Ni(CO)x species of the Mn promoted Ni catalyst leads to suppressing sintering of nickel particles [11, 24], as proved by XRD and TEM, contributing to the good stability during CO methanation.

The kinetic study on CO methanation (Fig. S4) was performed to explore the apparent activation energy (Ea) of 10%Ni/SiO$_2$ and 4%Mn-10%Ni/SiO$_2$ catalysts in the range of 270 °C − 280 °C. The Ea value of 4%Mn-10%Ni/SiO$_2$ was calculated to be 73.1 kJ/mol according to Arrhenius equation, much lower than that of 10%Ni/SiO$_2$ catalyst as 139.1 kJ/mol. Therefore, the addition of Mn onto Ni/SiO$_2$ catalyst dramatically enhances the activity of the obtained catalyst for CO methanation reaction, as proved by in-situ CO-DRIFTS.

The spent catalysts were characterized by TGA to analyze the carbon deposition of various catalyst. As shown in Fig. 6. The weight loss of 10%Ni/SiO$_2$ catalyst is the lowest due to its lowest CO conversion. For the Mn promoted catalysts, the weight loss increases with the increased Mn loading, indicating that the added Mn
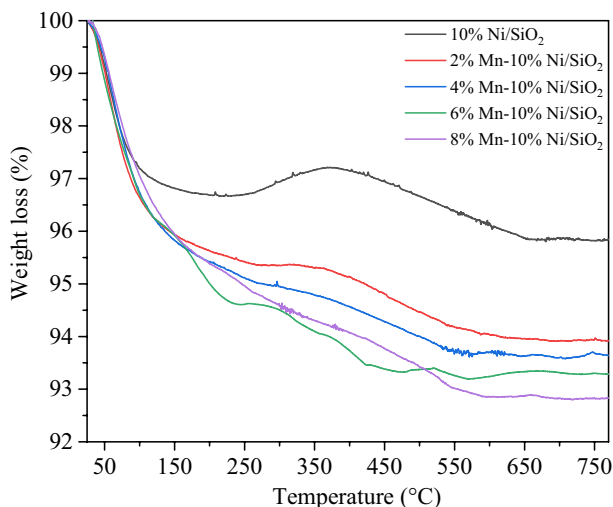
Fig. 6 TGA curves of the various used Ni/SiO$_2$ with different Mn loading. Operating conditions: 25 °C to 800 °C under air flow

might accelerate the carbon deposition during the methanation reaction because the NiCx species were found on the spent 8%Mn-10%Ni/SiO$_2$ catalysts as illustrated by XPS in Fig. 4b. Therefore, the 8%Mn-10%Ni/SiO$_2$ catalyst exhibited relatively bad stability than 4%Mn-10%Ni/SiO$_2$ catalyst, as shown in Fig. 1.

Conclusions

The Mn promoted Ni catalysts were developed and applied in CO methanation reaction. The added Mn significantly improves the dispersion of the supported nickel, suppresses the sintering of nickel particles and forms more adsorbed CO species of three-fold carbonyl species, resulting in higher CO conversion and good stability during CO methanation reaction. Meanwhile, the higher amount adsorbed CO species of three-fold carbonyl species on the Mn promoted catalysts would improve the selectivity of C$_2$+hydrocarbon. Besides, the lower ratio of Ni(CO)x species of the Mn promoted Ni catalyst leads to suppressing sintering of nickel particles. Base an the TGA and XPS results of the spent catalysts, the higher amount of added Mn would form NiCx species leading to deactivation.

Declarations

Conflict of interest The authors declare that they have no known competing financial interests or personal relationships that could have appeared to influence the work reported in this paper.

References

1. Hu DC, Gao JJ, Ping Y, Jia LH, Gunawan P, Zhong ZY, Xu GW, Gu FN, Su FB (2012) Enhanced Investigation of CO Methanation over Ni/Al_2O_3 catalysts for synthetic natural gas production. Ind Eng Chem Res 51:4875–4886
2. Wang H, Fang YZ, Liu Y, Bai X (2012) Perovskite $LaFeO_3$ supported bi-metal catalyst for syngas methanation. J Nat Gas Chem 6:745–752
3. Barrientos J, Lualdi M, Boutonnet M (2014) Deactivation of supported nickel catalysts during CO methanation. Appl Catal A 486:143–149
4. Italiano C, Llorca J, Pino L, Ferraro M, Antonucci V, Vita A (2020) CO and CO_2 methanation over Ni catalysts supported on CeO_2, Al_2O_3 and Y_2O_3 oxides. Appl Catal B: Environ 264:118494
5. Lin XH, Yang K, Si RR, Chen X, Dai WX, Fu XZ (2014) Photo-assisted catalytic methanation of CO in H_2-rich stream over Ru/TiO_2. Appl Catal B 147:585–591
6. Liu JX, Su HY, Li WX (2013) Structure sensitivity of CO methanation on Co (0001), (1012) and (1120) surfaces: density functional theory calculations. Catal Today 215:36–42
7. Weatherbee GD, Bartholomew CH (1982) Hydrogenation of CO_2 on group VIII metals: II. Kinetics and mechanism of CO_2 hydrogenation on nickel. J Catal 77:460–472
8. Guo X, Traitangwong A, Hu M, Zuo C, Meeyoo V, Peng Z, Li C (2018) Carbon dioxide methanation over nickel-based catalysts supported on various mesoporous material. Energy Fuels 32:3681–3689
9. Aziz MAA, Jalil AA, Triwahyono S, Mukti RR, Taufiq-Yap YH, Sazegar MR (2014) Highly active Ni-promoted mesostructured silica nanoparticles for CO_2 methanation. Appl Catal B: Environ 147:359–368
10. Aziz MAA, Jalil AA, Triwahyono S, Ahmad A (2015) CO_2 methanation over heterogeneous catalysts: recent progress and future prospects. Green Chem 17:2647–2663
11. Chen Y, Qiu B, Liu Y, Zhang Y (2020) An active and stable nickel-based catalyst with embedment structure for CO_2 methanation. Appl Catal B: Environ 269:118801
12. Hu CW, Yao J, Yang HQ, Chen Y, Tian AM (1997) On the inhomogeneity of low nickel loading methanation catalyst. J Catal 166:1–7
13. Hwang S, Lee J, Hong UG, Seo JG, Jung JC, Koh DJ, Lim H, Byun C, Song IK (2011) Methane production from carbon monoxide and hydrogen over nickel–alumina xerogel catalyst: effect of nickel content. J Ind Eng Chem 17:154–157
14. GaoJ JC, Li J, Zhang M, Gu F, Xu G, Zhong Z, Su F (2013) Effect of nickel nanoparticle size in $Ni/\alpha-Al_2O_3$ on CO methanation reaction for the production of synthetic natural gas. Catal Sci Technol 3:2009–2015
15. Munnik P, Velthoen ME, de Jongh PE, de Jong KP, Gommes CJ (2014) Nanoparticle growth in supported nickel catalysts during methanation reaction—larger is better. Angew Chem Int Ed 126:9647–9651
16. Deleitenburg C, Trovarelli A (1995) Metal-support interactions in Rh/CeO_2, Rh/TiO_2, and Rh/Nb_2O_5 catalysts as inferred from CO_2 methanation activity. J Catal 156:171–174
17. Vannice MA, Wang SY, Moon SH (1981) The effect of SMSI (strong metal-support interaction) behavior on CO adsorption and hydrogenation on Pd catalysts: I. IR spectra of adsorbed CO prior to and during reaction conditions. J Catal 71:152–166
18. AzizMAA JAA, Triwahyono S, Sidik SM (2014) Methanation of carbon dioxide on metal-promoted mesostructured silica nanoparticles. Appl Catal A 486:115–122
19. Qin Z, Ren J, Miao M, Li Z, Lin J, Xie KC (2015) The catalytic methanation of coke oven gas over $Ni-Ce/Al_2O_3$ catalysts prepared by microwave heating: Effect of amorphous NiO formation. Appl Catal B: Environ 164:18–30
20. Li XC, Hu QH, Yang YF, Wang Y, He F (2012) Studies on stability and coking resistance of $Ni/BaTiO_3–Al_2O_3$ catalysts for lower temperature dry reforming of methane (LTDRM). Appl Catal A: Gen 413:163–169

21. Lv X, Chen JF, Tan Y, Zhang Y (2012) A highly dispersed nickel supported catalyst for dry reforming of methane. Catal Commun 20:6–11
22. Agnelli M, Kolb M, Mirodatos C (1994) Co Hydrogenation on a nickel catalyst: 1. Kinetics and modeling of a low-temperature sintering process. J Catal 148:9–21
23. Shen WM, Dumesic JA, Hill CG (1981) Criteria for stable Ni particle size under methanation reaction conditions: nickel transport and particle size growth via nickel carbonyl. J Catal 68:152–165
24. Bai YX, Zhang JF, Yang GH, Zhang QD, Pan JX, Xie HJ, Liu XC, Han YZ, Tan YS (2018) Insight into the nanoparticle growth in supported Ni catalysts during the early stage of CO hydrogenation reaction: the important role of adsorbed CO molecules. ACS Catal 8:6367–6374
25. Younas M, Kong LL, Bashir MJK, Nadeem H, Shehzad A, Sethupathi S (2016) Recent advancements, fundamental challenges, and opportunities in catalytic methanation of CO_2. Energy Fuels 30:8815–8831
26. Beierlein D, Häussermann D, Pfeifer M, Schwarz T, Stöwe K, Traa Y, Klemm E (2019) Is the CO_2 methanation on highly loaded Ni-Al_2O_3 catalysts really structure-sensitive. Appl Catal B: Environ 247:200–219
27. Wu HC, Chang YC, Wu JH, Lin JH, Lin IK, Chen CS (2015) Methanation of CO_2 and reverse water gas shift reactions on Ni/SiO_2 catalysts: the influence of particle size on selectivity and reaction pathway. Catal Sci Technol 5:4154–4163
28. Liu J, Li CM, Wang F, He S, Chen H, Zhao YF, Wei M, Evans DG, Duan X (2013) Enhanced low-temperature activity of CO_2 methanation over highly-dispersed Ni/TiO_2 catalyst. Catal Sci Technol 3:2627–2633
29. Zhou WG, Liu JY, WuX CJF, Zhang Y (2015) An effective Co/MnOx catalyst for forming light olefins via Fischer-Tropsch synthesis. Catal Commun 60:76–81
30. Liu Y, Chen JF, Bao J, Zhang Y (2015) Manganese-modified Fe3O4 microsphere catalyst with effective active phase of forming light olefins from syngas. ACS Catal 5:3905–3909
31. Morales F, de Groot FMF, Gijzeman OLJ, Mens AD, Stephan O, Weckhuysen BM (2005) Mn promotion effects in Co/TiO_2 Fischer-Tropsch catalysts as investigated by XPS and STEM-EELS. J Catal 230:301–308
32. Feltes TE, Espinosa-Alonso L, de Smit E, D'Souza L, Meyer RJ, Weckhuysen BM, Regalbuto JR (2010) Selective adsorption of manganese onto cobalt for optimized Mn/Co/TiO_2 Fischer-Tropsch catalysts. J Catal 270:95–102
33. Choudhury MBI, Ahmed S, Shalabi MA, Inui T (2006) Preferential methanation of CO in a syngas involving CO_2 at lower temperature range. Appl Catal A: Gen 314:47–53
34. Jia X, Zhang X, Rui N, Hu X, Liu CJ (2019) Structural effect of Ni/ZrO_2 catalyst on CO_2 methanation with enhanced activity. Appl Catal B: Environ 244:159–169
35. Wang Y, Yao L, Wang YN, Wang SH, Zhao Q, Mao DH, Hu CW (2018) Low-temperature catalytic CO_2 dry reforming of methane on Ni-Si/ZrO_2 catalyst. ACS Catal 8:6495–6506
36. Czekaj I, Loviat F, Raimondi F, Wambach J, Biollaz S, Wokaun A (2007) Characterization of surface processes at the Ni-based catalyst during the methanation of biomass-derived synthesis gas: X-ray photoelectron spectroscopy (XPS). Appl Catal A: Gen 329:68–78
37. Liu Y, Sheng W, Hou ZG, Zhang Y (2018) Homogeneous and highly dispersed Ni–Ru on a silica support as an effective CO methanation catalyst. RSC Adv 8:2123–2131
38. Yan Y, Dai Y, Yang Y, Lapkin AA (2018) Improved stability of Y_2O_3 supported Ni catalysts for CO_2 methanation by precursor-determined metal-support interaction. Appl Catal B: Environ 237:504–512
39. Vogt C, Groeneveld E, Kamsma G, Nachtegaal M, Lu L, Kiely C, Berben P, Meirer F, Weckhuysen B (2018) Unravelling structure sensitivity in CO_2 hydrogenation over nickel. Nat Catal 1:127–134